THE IMPACT OF FERROFLUID ACTUATED BY AN EXTERNAL MAGNETIC FIELD ON HEAT EXCHANGE PERFORMANCES OF CURVED CHANNELS

Cuihua Wang, Jiaxu Sui, Xinhao Wang, Xianzhen Zhang, Peng Liu, Bin Gong *

School of Mechanical and Power Engineering, Shenyang University of Chemical Technology, Shenyang, China

* Corresponding author; E-mail: yjs_0505@163.com

The development rules of ferrofluid flow and heat exchange in curved channels under the influence of external magnetic field were thoroughly investigated using the finite element method. The comprehensive strengthening performance of elbows under magnetic fields was evaluated based on the factors including the dimensionless pressure coefficient, heat transfer coefficient, and comprehensive strengthening factor. The results demonstrate that the heat transfer coefficient can be improved by increasing the volume fraction of ferrofluid in the presence of lower or no magnetic field, while it exhibits no significant variation with the increase of the volume fraction for higher magnetic fields. For a given volume fraction, a lower magnetic field may slightly inhibit heat transport of ferrofluid. A higher magnetic field can induce a complex swirling flow of the fluid along the curved axis. As the curvature decreases, the magnetic field effect becomes stronger, leading to the coupling of the magnetic field force with the centrifugal force. This coupling results in three pairs of secondary vortices on the cross-section and the heat exchange capacity is significantly enhanced. Within the study, the heat transfer coefficient of the curved tube with a dimensionless curvature of 0.067 for the magnetic field intensity of 1800G increased by 43.51%, and the comprehensive strengthening factor is 1.326, compared to without a magnetic field.

Key words: *magnetic field, curved channel, ferrofluid, heat transfer enhancement*

1. Introduction

With the rapid development of energy, electronics and artificial intelligence, the problem that the devices with high heat flux density being unable to dissipate heat quickly has seriously affected the performance, reliability, and service life of many new types of equipment. In addition, there are also cooling problems under extreme conditions. Traditional working fluids can no longer meet the above requirements. Ferrofluid has great development potential in the fields of efficient energy transfer and controllable one, because of its superior heat transfe and controllability by external magnetic field, which brings new opportunities for highly efficient heat exchange on electronic cooling, nuclear reactors and so on [1-5].

Researchers conducted a comparative analysis of the heat exchange characteristics of ferrofluid in the absence and presence of an external magnetic field. Bijarchi *et al*. [6] discussed the

experimental study on the generation of magnetic fluid droplets by magnetic field in microfluidics. They found that increasing the magnetic field strength can increase the droplet diameter and generation frequency. It can further promote the application of microfluidic technology in biomedicine, chemical reaction and material synthesis. Wiriyasart *et al*. [7] experimentally studied the thermal performance of thermoelectric cooling module of compact radiator with water, nanofluid and ferrofluid as coolants. They reported that the heat exchange performance of Fe_3O_4 ferrofluid surpassed both water and TiO_2 nanofluid, with a maximum heat exchange efficiency exceeding that of TiO_2 nanofluid by 11.17% and water by 12.57%. Bezaatpour *et al*. [8] put forward an efficient method to improve the hydrothermal and exergetic performance of heat exchangers. They found that heat exchange efficiency can improved by generating a swirl in the tube by using a magnetic field, achieving an enhancement of up to 90%. Within the research scope of Goharkhah *et al*. [9], it was discovered that the average convective heat transfer increased by 13.5% with a 2% ferrofluid volume fraction in the absence of an external magnetic field. Whereas, the heat exchange rate was significantly enhanced upon the actuation of an external magnetic field. Li *et al*. [10] found that the use of nanofluids can significantly reduce the chip temperature and improve the convective heat transfer coefficient compared with deionized water. This effect is more obvious under the action of magnetic field. It also provides an experimental basis for the application potential of nanofluids in the field of thermal management. Bennia *et al*. [11] elucidated the heat exchange mechanism of magnetic nanofluids in the presence of coupled fluid-magnetic forces. Their findings indicated that the Nusselt number increased with an increase in the volume fraction of nanoparticles and the presence of a magnetic field. Asfer *et al*. [12] conducted a bright-field visualization study focusing on nanoparticle clusters and aggregation patterns on the inner wall of stainless-steel tubes. They thought the increase or decrease of the convective heat transfer coefficient of ferrofluid in the presence of an external magnetic field was attributed to three factors: the ratio of magnetic force to inertial force on ferrofluid; Interaction of nanoparticle aggregates; The strengthening of local thermal conductivity resulted from nanoparticle chains.

Based on current research, the flow behavior of ferrofluids is influenced by the microstructure and migration patterns of nanoparticles. Notably, the enhanced heat exchange mechanism of ferrofluids actuated by an external magnetic field is notably more intricate than those observed in the absence of a magnetic field. Presently, the theoretical research on this enhanced heat transfer behavior is still being developed and requires further exploration and improvement.

To enhance heat exchange capabilities, ferrofluid serves as a passive approach, while the utilization of curved channels has been another prevalent method. Due to space constraints, curved ducts have been extensively used in various environments to connect straight pipes. The improvement in heat exchange within curved ducts has been attributed to the formation of Dean vortices, which intensifies fluid inhomogeneity and instability [13]. Researchers usually employ the Dean number ($Dn= Re\sqrt{K}$, where K represents the dimensionless curvature of the curved channels) to predict fluid flow characteristics. Hence, the flow characteristics of the ducts are significantly influenced by the curvature. The flow direction of fluid is changed with different curvatures, leading to flow separation within the channel, which changed the magnitude of centrifugal force, thus the different rules about flow and heat exchange are generated.

When a magnetic field is applied to ferrofluids flowing through curved channels, magnetic field forces are generated. The flow behavior is altered by the coupling of the magnetic field force and

centrifugal force, resulting in increasingly intricate flow field structures and heat transfer characteristics. Akar *et al*. [14] observed that the blood flow in 90° curved blood vessels was disturbed under a high magnetic field, leading to fluctuations in wall shear stress distribution. Vafeas *et al*. [15] demonstrated that the magnetic field significantly impacted the velocity distribution of ferrofluid flow in a 90° curved annular pipe. The effect of secondary flow in the channel was remarkable after exerting a magnetic field. Their research provides a theoretical basis and guidance for the flow control of magnetic fluid in engineering applications, especially when designing compact and efficient heat exchangers and mixers. Bakalis *et al*. [16] studied the laminar magnetohydrodynamic (MHD) flow of liquid metal in a curved pipe, considering the influence of transverse external magnetic field. Their research on MHD flow in complex geometric structures (such as curved pipes) provides an important numerical analysis method, which is of great significance to thermal management and hydrodynamic design in fusion reactors and other engineering applications.

In summary, the related research on the composite strengthening technology of ferrofluid-magnetic field-bending duct is insufficient. Limited research has been conducted on how the flow and heat exchange properties of ferrofluids are altered by the magnetic field applied on curved tubes. Based on this, the comprehensive strengthening performance of elbow under magnetic field is evaluated from dimensionless pressure coefficient, heat transfer coefficient and comprehensive strengthening factor. The effects of curvature, magnetic field intensity and volume fraction on the flow and heat transfer of ferrofluid in the elbow are emphatically discussed. Thus, it lays a theoretical foundation for the application of this composite strengthening technology in heat exchangers.

2. Numerical simulation

2.1. Model geometry

The geometrical model of a copper bent pipe with a 1mm wall thickness used in the numerical simulations is illustrated in Fig. 1. The inner radius of the bent pipe is Rp = 10 mm and the Rc is the radius of the bent axis. The dimensionless curvature is determined using the formula K=Rp/Rc. The entrance and exit are each extended by 5D. The bent pipe is placed in the gap of an electromagnet (seen in Fig. 2) and it generates a uniform magnetic field in the Z-direction, which is applied to the ferrofluid flowing through the duct. For additional information on electromagnets, please refer to Reference [17].

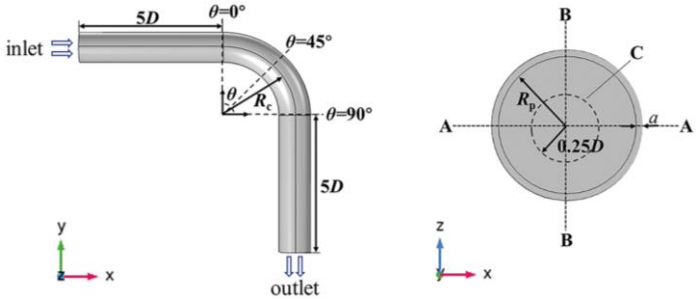

Figure 1. The geometric model

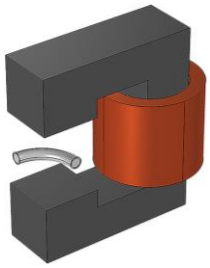

Figure 2. The electromagnet and bend pipe

2.2. Control equations

Assuming steady state condition, the nanofluid is uniform and the viscous dissipation and chemical reaction inside the nanofluid are ignored. The governing equations can be given as follows[18]:

$$\nabla \cdot (\rho V) = 0 \tag{1}$$

$$\nabla \cdot (\rho VV) = -\nabla p + \nabla \cdot (\tau_{ij}) + F_M \tag{2}$$

$$\nabla \cdot (\rho VC_p T) = \nabla \cdot (k \nabla T) \tag{3}$$

V is the velocity vector, τ_{ij} is the shear tensor.

$$\tau_{ij} = \mu(\partial V_i / \partial X_j + \partial V_j / \partial X_i) - 2/3 \mu \delta_{ij} (\partial V_i / \partial X_i) \tag{4}$$

To simplify the mathematical model and calculation process, the ferrofluid is considered to be non-conductive to avoid current passing through the fluid, which will lead to additional heat loss or electromagnetic effect [19]. The magnetic field force is the following:

$$F_M = \frac{1}{2} \mu_0 \chi_m (1 + \chi_m) \nabla (H \cdot H) + \mu_0 \chi_m H ((H \cdot \nabla) \chi_m) \tag{5}$$

There is a uniform magnetic field (Z-direction) and zero magnetic field gradient. Thus, the magnetic source term F_M can be simplified as:

$$F_M = \mu_0 \chi_m H \frac{-\chi_0 \beta H_z}{[1 + \beta (T - T_0)]^2} \frac{\partial T}{\partial z} \tag{6}$$

Please refer to the literature[20] for a detailed derivation of the formula of magnetic field force.

2.3. Thermophysical properties

The equations of nanofluid density, specific heat, viscosity, and thermal conductivity are written as [21]:

$$\rho_{nf} = (1 - \Phi)\rho_f + \Phi \rho_{np}, Cp_{nf} = \frac{(1 - \Phi)\rho_f Cp_f + \Phi \rho_{np} Cp_{np}}{\rho_{nf}} \tag{7}$$

$$\mu_{nf} = \mu_f (1 + 2.5\Phi) \ \ \Phi \le 2\%, \mu_{nf} = \frac{\mu_f}{(1 - \Phi)^{2.5}} \ \ \Phi > 2\% \tag{8}$$

Where, subscripts f, np and nf represent basic fluid, nanoparticles and nanofluids. The physical properties of solid nanoparticles are assumed to be constant. k_{np}=7 W/(m·K), ρ_{np}=4950 kg/m^3, D_{np}=20 nm and Cp_{np}=640 J/(kg·K). The thermal conductivity is calculated using Koo and Kleinstreuer correlation [19].

$$k_{\mathrm{nf}} = k_{\mathrm{f}}\left[\frac{(k_{\mathrm{np}}+2k_{\mathrm{f}})-2\Phi(k_{\mathrm{f}}-k_{\mathrm{np}})}{(k_{\mathrm{np}}+2k_{\mathrm{f}})+\Phi(k_{\mathrm{f}}-k_{\mathrm{np}})}\right]+5\times10^{4}\,\vartheta\Phi\rho_{\mathrm{f}}Cp_{\mathrm{f}}\sqrt{\frac{\gamma T}{\rho_{\mathrm{np}}D_{\mathrm{np}}}}g(\Phi,T) \tag{9}$$

Where, $\gamma = 1.38\times10^{-23}$ J/K is the Boltzmann constant. The correction functions of $g(\Phi, T)$ and ϑ are given by:

$$g(\Phi,T) = (-6.04\Phi + 0.4705)T + 1722.3\Phi - 134.63 \tag{10}$$

$$\vartheta = -0.673\Phi^{3} + 0.2452\Phi^{2} - 0.01782\Phi + 0.000487 \quad 1\% \le \Phi \le 4\% \tag{11}$$

The base fluid physical property as a function of temperature can be calculated as follows [22]:

$$\begin{aligned}\rho_{\mathrm{f}} &= 2446 - 20.674T + 0.11576T^{2} - 3.12895\times10^{-4}T^{3} \\ &\quad + 4.0505\times10^{-7}T^{4} - 2.0546\times10^{-10}T^{5}\end{aligned} \tag{12}$$

$$\mu_{\mathrm{f}} = 2.414\times10^{-5}\times10^{[\frac{247.8}{T-140}]} \tag{13}$$

$$k_{\mathrm{f}} = -1.13 + 9.71\times10^{-3}T - 1.31\times10^{-5}T^{2} \tag{14}$$

2.4. Data processing

The average heat transfer coefficient h_{ave}, the dimensionless axial velocity U^{*}, the dimensionless temperature T^{*}, the coefficient of frictional resistance f, the Reynolds number Re, and the comprehensive strengthening factor η are defined as follows:

$$h_{\mathrm{ave}} = \frac{q_{\mathrm{w}}}{T_{\mathrm{W}} - T_{\mathrm{nf}}},\ U^{*} = \frac{U}{U_{ave}},\ T^{*} = \frac{(T - T_{\mathrm{in}})k_{\mathrm{nf}}}{q_{\mathrm{w}}D} \tag{15}$$

$$f = \frac{\Delta p}{(\rho_{\mathrm{nf}}U_{\mathrm{in}}{}^{2}/2)(l/D)},\ Re = \frac{U_{\mathrm{in}}\rho_{\mathrm{nf}}D}{\mu_{\mathrm{nf}}},\ \eta = \frac{h_{\mathrm{nf}}/h_{\mathrm{f}}}{(f_{\mathrm{nf}}/f_{\mathrm{f}})^{1/3}} \tag{16}$$

3. Boundary conditions, methodology and validation

The simulation is carried out by Comsol software in this paper. A constant heat flux is applied on the outer surface of the channel. Considering that the normal temperature medium is between 293 K and 303 K, a ferrofluid with the inlet temperature T_{in}=294K is chosen for subsequent calculation of the bend tube. The inlet is defined as uniform velocity, the outlet is atmospheric pressure and the no-slip condition is used to the inner surface. The solution is carried out using the finite element discretization method with the above assumptions and boundary conditions. PARDISO and GMRES solver is chosen to calculate flow module and heat transfer module respectively and the convergence residual is set below 10^{-6}. A structured non-uniform mesh is used for the simulations, and the mesh refinement is specifically focused on regions including bends and near-wall areas that large temperature and velocity gradients. The grid distribution is showed in Fig. 3.

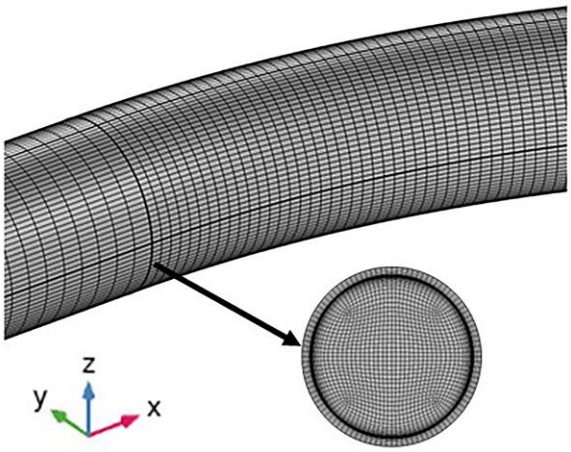

Figure 3. Grid division

The h_{ave} and f values for mesh numbers of 239054, 321846, 435448 and 586496 are calculated at Re=1500 and Rc=150 mm and the relative differences from the previous mesh results are given in Tab. 1. It is observed that after increasing the grids number to 586496, the grid refinement had little impact on the calculation results. Ultimately, the 435448 grids were chosen for simulations in consideration of the computational time and accuracy.

Table 1. Grid-independent verification

Grids	h_{ave}(W/m^{2}K)	Error	f (×10^{-3})	Error
239054	1156.76	-	80.940	-
321846	1157.59	0. 072%	81.138	0. 245%
435448	1156.90	-0. 060%	81.211	0. 090%
586496	1156.38	-0.045%	81.192	-0.023%

The experimental results and numerical simulation results (heat transfer coefficient h and pressure drop Δp) of ferrofluid in straight tubes under an external magnetic field are shown in Fig. 4(a) and Fig. 4(b). The flow and heat transfer of magnetic nanofluid in a circular channel with T_{in}=333 K and B=800G were simulated, and the results were compared with the experimental data of Sha *et al.* [23]. The simulation data are in good agreement with the experimental data, with the same trend and the error is within 5%. The simulation results using the same numerical model were very consistent with the results given in the literature [18]. Besides, their results have been verified by available experimental data.

The numerical simulation results and experimental results (dimensionless velocity U/U_{ave} and temperature T_{nf}) of ferrofluid in curved channels without external magnetic field are presented in Fig. 4(c) and Fig. 4(d). The flow of fluid in a curved duct with Re=1000 and K=0.18 was simulated, and the results are compared with those of Nicolaou *et al.* [24] and Taibi *et al.* [25] in the Fig. 4 (c), which is more consistent with Nicolaou's result. On the other hand, the flow and heat transfer of ferrofluid with T_{in}=283.65 K and Rc= 200 mm without magnetic field were simulated, and compared the results with the experimental results of Kelidari *et al.* [26]. From the Fig. 4(d), the simulation results have the same trend as the experimental data and the error is within 3%.

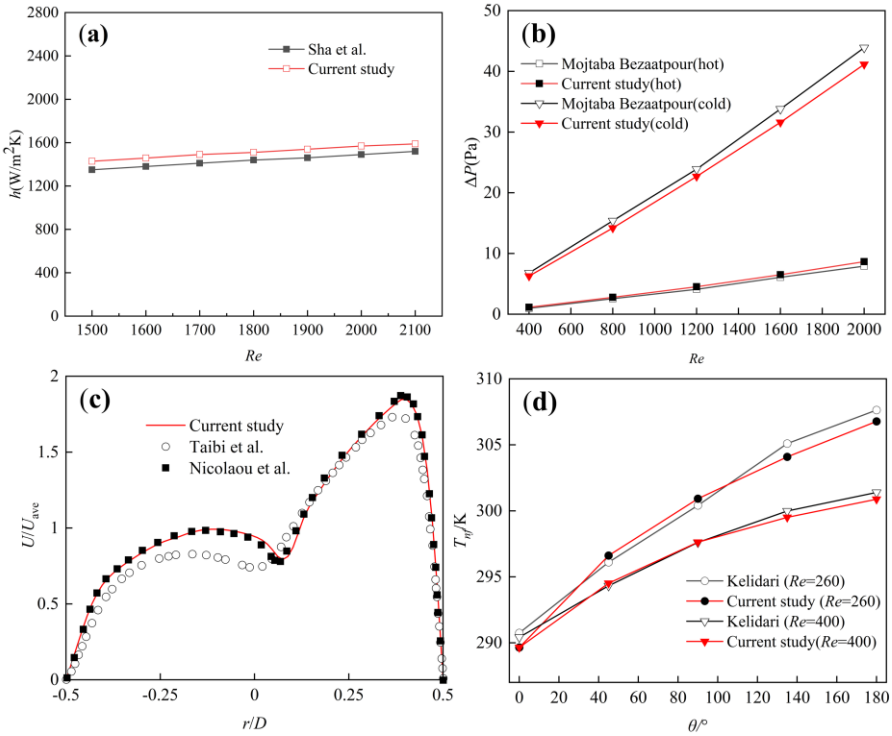

Figure 4. Numerical and experimental results for (a) heat transfer coefficient (b) pressure drop (c) dimensionless axial velocity and (d) temperature T_{nf}

4. Results and discussion

4.1. The effect of Φ on heat transfer performances of curved pipes

As depicted in Fig. 5, the magnetic nanofluid employed within the curved channel exhibits a higher heat transfer coefficient compared to deionized water. The convective heat transfer coefficient of Φ=3% ferrofluid is increased by 8.23% compared to deionized water at Re=800. The heat transfer coefficient of the curved channel improves with the increase in the volume fraction of the nanofluid. whereas, when Φ>1.5%, the heat transfer coefficient is slightly affected by Φ. This trend is attributed to the interaction between thermal conductivity and viscosity, which is consistent with the research results of Sha *et al.* [27]. As the Φ increases, the Brownian motion of nanoparticles is intensified, which increases the thermal conductivity of ferrofluid. However, the viscosity increases as well, which diminishes the positive impact of high thermal conductivity on heat exchange.

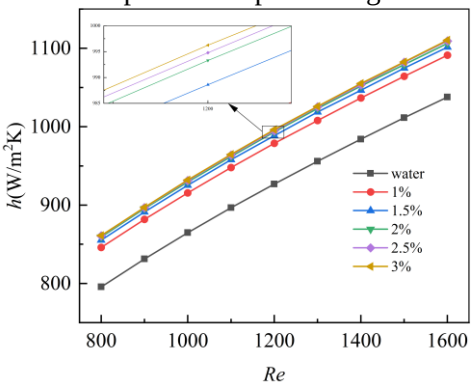

Figure 5. Variation of heat transfer coefficient with Re for different Φ (K=0.067)

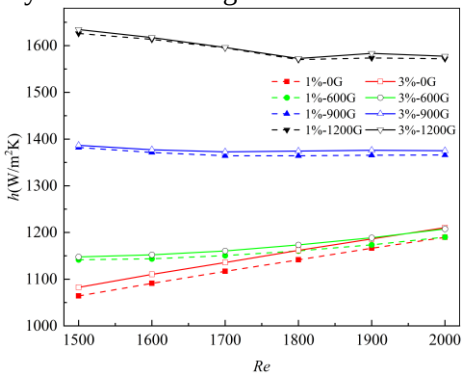

Figure 6. Variation of h with Re for different B and Φ(K=0.067)

The heat transfer coefficients of ferrofluid with different volume fractions applied external magnetic fields are compared in Fig. 6. It is observed that an increase in volume fraction leads to an improvement in the heat transfer coefficient of the curved duct in the absence of a magnetic field and lower magnetic field intensities. However, as *B* increases, the enhancement in heat exchange is little affected by the increase of volume fraction. Consequently, a ferrofluid with a volume fraction of 3% is chosen as the flow medium for subsequent analysis of the curved tube.

4.2. The effect of *K* and *B* on heat transfer performances of curved pipes

4.2.1 Analysis of Flow Characteristics

Effect of magnetic field on the cross sectional pressure variation in the curved channel is demonstrated in Fig 7. The pressure distributions on the cross sections of the bends with different curvatures are similar when there is no magnetic field action. Due to the centrifugal force, the fluid is thrown toward the outer wall of the tube, resulting in a high-pressure zone near the outer wall and a low-pressure zone near the inner wall. The pressure value gradually increases from inner to outer along the radial direction. Whereas, the fluid is subjected to both centrifugal force and magnetic field force in the presence of an external magnetic field. The coupling action of two forces makes pressure gradient on the cross-section not only exist along the radial direction and the larger the *B* value or the smaller the *K* value, and the more multi-directional the pressure gradient on the cross-section.

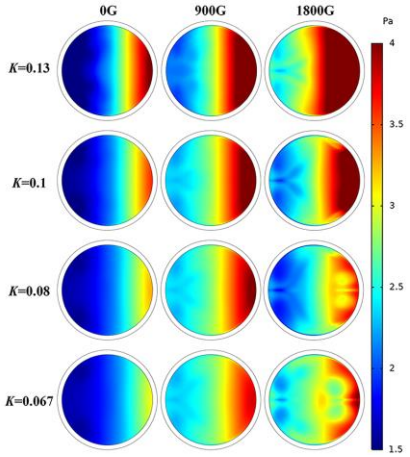

Figure 7. Pressure distribution with different *B* and *K* (*Re*=2500, *θ*= 90°)

To further investigate the variation of local pressure on the cross-section, Fig. 8 gives the relative pressure on the C-line (it is location as shown in Fig. 1) in the cross-section. Here, $C_{pre}=(p-p_{in})/(0.5\rho U^2)$ represents the dimensionless pressure coefficient [28]. As depicted in Fig. 8, a smoother curve indicates a more regular pressure distribution in the radial direction. Furthermore, a decrease in the area enclosed by the curve signifies a lower relative pressure. When *B*=0G, the fluid is only droven by centrifugal force, and the pressure distribution shows a pattern of "higher near outer side and lower near inner side". With increasing *B* or decreasing *K*, the pressure field within the channel becomes more complex, resulting in a less smooth curve. At *K*=0.067 and *B*=1800G, the pressure along the C-line exhibits the greatest nonuniformity, with the relative pressure reaching its minimum value.

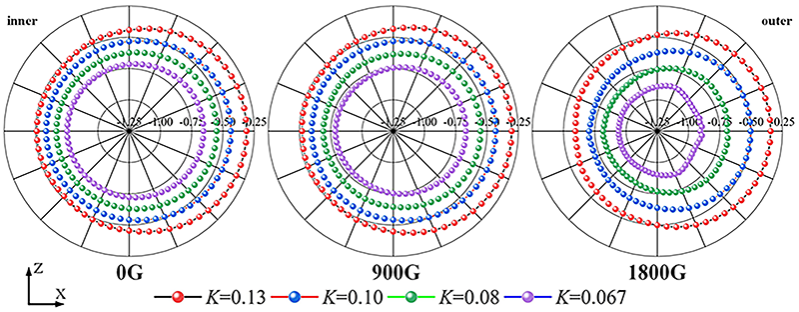

Figure 8. Pressure distribution on line C of different *B* and *K* (*Re*=2500, *θ*= 90°)

Figure 9 illustrates the velocity streamline diagram in the bend for the conditions of K=0.067 and B=1800 G. With the development of flow, the ferrofluid in the diagram is actuated by both the magnetic field force and centrifugal force, which results in an alteration of the pressure field in the curved channel, and a complex swirling flow along the curved axis is occured.

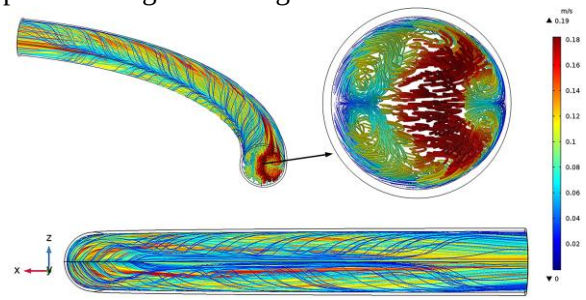

Figure 9. The velocity streamline (*B*=1800G, *Re*=2500, *K*=0.067)

Figures 10 and 11 give the comparison of the dimensionless axial velocity (U^*) and secondary flow vector on the θ=90° cross-section for varying values of B and K respectively. As depicted in Fig. 10, the high axial velocity region of the fluid is close to the outer wall for B=0 G. Upon the application of an external magnetic field, a symmetric region of lower velocity appears near the outer wall, with the high-speed region gradually moving towards the center of the cross-section. Furthermore, the smaller the curvature K, the larger the range of the low-speed area near the outer wall, the narrower the high-speed region, and the greater the maximum axial velocity value.

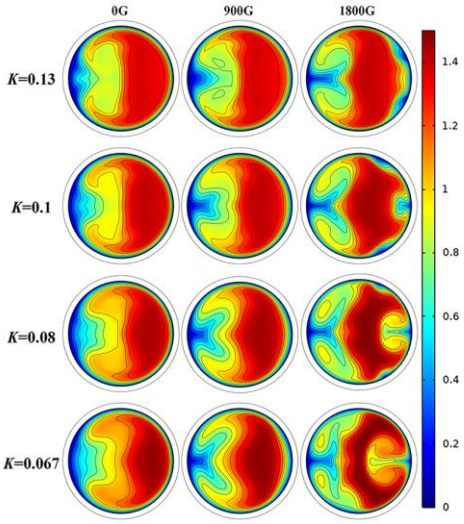

Figure 10. Distribution of dimensionless axial velocity for different *B* and *K* (*Re*=2500, *θ*= 90°)

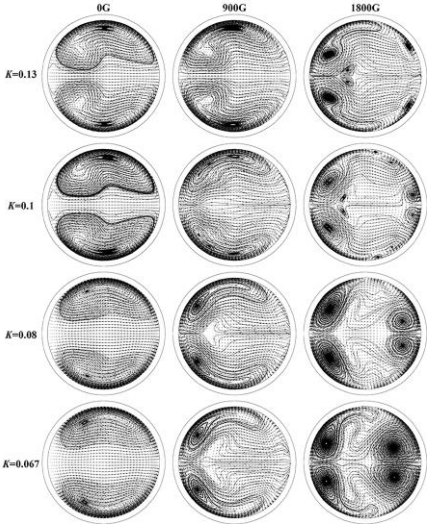

Figure 11. Comparison of secondary flow vectors for different *B* and *K* (*Re*=2500, *θ*= 90°)

As shown in Fig. 11, due to the existence of curvature in the bent tube at B=0G, there are two opposing secondary centrifugal vortices on the cross-section and the larger K, the stronger the centrifugal vortices and the larger the range of the centrifugal vortices. Upon the application of a magnetic field, the centers of the two centrifugal vortices gradually shift towards the inner end of the A-A centerline along the upper and lower walls, respectively. As B increases, two pairs of additional vortices flowing in opposite direction to the centrifugal vortices gradually appear on the upper and lower sides of the A-A centerline. Notably, the additional vortices are more intense for smaller K. Combining the pressure distribution in Fig. 7 and mainstream velocity distribution in Fig. 10 given above, it can be revealed that the central regions of the three pairs of secondary vortices have lower axial velocity and pressure.

The results above suggest that a compound swirling flow is formed due to the combined action of the strong magnetic field force and centrifugal force, which distroys the boundary layer, enhances the mixing of ferrofluid in the curved channel, and ultimately strengthens heat transfer.

4.2.2 Analysis of Enhanced heat transfer Performance

Figures 12 and 13 depict the variations of the cross-sectional average heat transfer coefficient h_{ave} along θ and the total heat transfer coefficient h with the curvature and the magnetic intensity respectively. For B=0G, the heat transfer coefficient h of the elbow with K=0.13 is increased by 24.57% compared to the duct with K=0.067. Therefore, heat transfer of the elbow can be significantly enhanced by an increment in the curvature when there is no exernal magnetic field. In this case, the use of bends with greater curvature is desirable, taking into account the enhanced heat transfer in practical engineering applications. In addition, in the absence of magnetic field, the research results are compared with those of Fadaei *et al*. [29], and a similar conclusion is obtained. As the fluid flows forward along the pipe, the heat transfer coefficient tends to decrease gradually. The h_{ave} of the cross section when B =1800G is significantly higher than the h_{ave} of the cross section at the same location when B= 0G, with the exception of the region near the entrance where the magnetic field force is minimal, resulting in a negligible impact on heat transfer. Therefore, when B=1800G the h of the four curved pipes compared to the absence of a magnetic field increased by 19.78%, 28.43%, 35.89%, and 43.51%. (seen from Fig. 13).

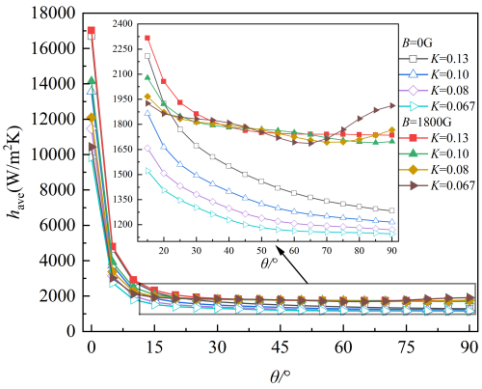

Figure 12. Variation of h_{ave} along the bending angle θ for different K (Re =2500)

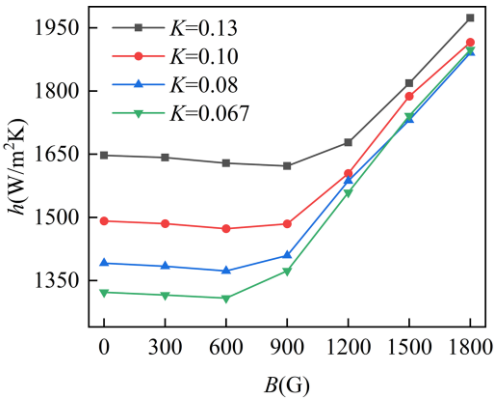

Figure 13. Variation of total heat transfer coefficient for different B and K (Re =2500)

Figure 14 depicts the variation in the comprehensive strengthening factor η with magnetic field strength and curvature. For a given K, the total heat transfer coefficient initially decreases slightly and then increases with an increase in B by analyzing Fig. 13 and Fig. 14. The η follows a similar trend.

Specifically, when B>600 G or B>900 G, the total heat transfer coefficient appears a significantly increase as B raises. In all cases, the η is more than 1. The heat transfer in the curved pipe is initially slightly inhibited for lower B, resulting in η values less than 1. Whereas, as B reaches a certain value, the combined effect of the stronger magnetic field force and centrifugal force generates a composite swirling flow that significantly enhances heat transfer and improves the comprehensive strengthening factor. Notably, the maximum comprehensive strengthening factor for the four curves is 1.326 when B=1800 G. The smaller the curvature, the better the magnetic field enhanced effect, and the smaller the B where η starts to be greater than 1.0. Therefore, in practical engineering applications, it is more suitable to apply stronger magnetic field to strengthen the heat transfer of curved pipe with smaller curvature.

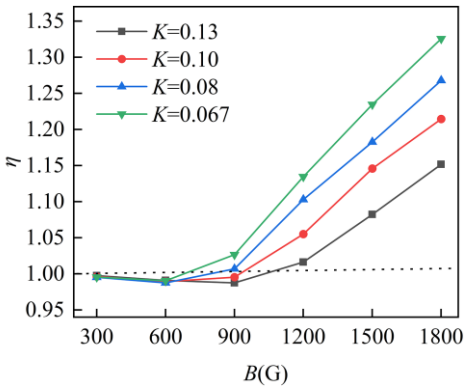

Figure 14. Variation of η for different B and K (Re =2500)

5. Conclusions

When the ferrofluid in curved channels actuated by an external magnetic field, it can be subjected to the combined action of magnetic field force and centrifugal force, and the coupling force changes the pressure field and velocity field inside the curved channel, resulting in complex swirling flow of the ferrofluid, and significantly enhancing heat transfer of the curved channel.

Curvature and magnetic field strength are important factors affecting heat transfer in curved pipes exerted an external magnetic field. The smaller the curvature, the better the heat transfer enhancement by the magnetic field with a constant B, and the lower the magnetic field strength that can enhance heat transfer.

For lower magnetic field intensity, the heat transfer of ferrofluid in four models is inhibited to a certain extent, and the comprehensive strengthening factor of curved channel is less than 1.0. However, when B>600 G or B>900 G, the total heat transfer coefficient is significantly improved, with all the comprehensive strengthening factors exceeding 1.0.

The heat transfer enhancement showed by ferrofluid in a 90° bend pipe is better under conditions of higher magnetic field strength and smaller curvature. In our study, the total heat transfer coefficient achieves a maximum increase of 43.51%, the comprehensive enhancement factor peaks at 1.326 when compared to the absence of a magnetic field.

Acknowledgment

This study was financially supported by the General Program of the Educational Department of Liaoning Province (Grants No. LJKZ0447, LJKMZ20220775)

Nomenclature

a	Thickness [mm]	U^*	axial relative velocity
B	magnetic flux density[$N \cdot A^{-1} \cdot m^{-1}$]	X, Y, Z	direction
C_P	specific heat [$kJ \cdot kg^{-1} \cdot K^{-1}$]	**Greek**	
D	inner diameter [mm]	μ_0	permeability of free space [$4\pi \times 10^{-7} N/A^2$]
f	resistance coefficient	θ	angle [0-90°]
F_M	Kelvin body force [N/m^3]	μ	dynamic viscosity [$N \cdot s/m^2$]
h	heat transfer coefficient [$W/m^2 \cdot K$]	χ_m	magnetic susceptibility
H	magnetic field intensity [$A \cdot m^{-1}$]	ρ	density [kg/m^3]
K	curvature	η	comprehensive strengthening factor
k	thermal conductivity [$W \cdot m^{-1} \cdot K^{-1}$]	β	thermal expansion coefficient [K^{-1}]
l	bending axis [mm]	Φ	volume fraction
p	pressure [Pa]	γ	Boltzmann constant [$1.38 \times 10^{-23} J \cdot K^{-1}$]
Rc	bent axis radius [mm]	**Subscripts**	
Re	Reynolds number	in	inlet
Rp	inner radius [mm]	nf	nanofluid
T	Temperature [K]	f	fluid
T_0	reference temperature 300[K]	np	nanoparticle
T^*	dimensionless temperature	w	wall
U	velocity [$m \cdot s^{-1}$]	ave	average

References

[1] Aglawe, K.R., *et al.*, Preparation, applications and challenges of nanofluids in electronic cooling: A systematic review, *Materials Today: Proceedings*, *43* (2021), pp. 366-372

[2] Bahiraei, M., *et al.*, Recent research contributions concerning use of nanofluids in heat exchangers: A critical review, *Applied Thermal Engineering*, *133* (2018), pp. 137-159

[3] Das, P., *et al.*, Recent advances in magnetic fluid hyperthermia for cancer therapy, *Colloids and Surfaces B: Biointerfaces*, *174* (2019), pp. 42-55

[4] Sharma, K.R., *et al.*, Review on using nanofluids for heat transfer enhancement in nuclear power plants, *Kerntechnik*, *83* (2018), pp. 426-438

[5] Ramalingam, S., *et al.*, Consequence of nanoparticles size on heat transfer characteristics of a radiator, *Powder Technology*, *367* (2020), pp. 213-224

[6] Bijarchi, M.A., *et al.*, Experimental investigation of on-demand ferrofluid droplet generation in microfluidics using a Pulse-Width Modulation magnetic field with proposed correlation, *Sensors and Actuators B-Chemical*, *329* (2021), 129274

[7] Wiriyasart, S., *et al.*, Heat transfer enhancement of thermoelectric cooling module with nanofluid and ferrofluid as base fluids, *Case Studies in Thermal Engineering*, *24* (2021), 100877

[8] Bezaatpour, M., Rostamzadeh, H., Energetic and exergetic performance enhancement of heat exchangers via simultaneous use of nanofluid and magnetic swirling flow: A two-phase approach, *Thermal Science and Engineering Progress*, *20* (2020), 100706

[9] Goharkhah, M., *et al.*, Convective heat transfer characteristics of magnetite nanofluid under the influence of constant and alternating magnetic field, *Powder Technology*, *274* (2015), pp. 258-267

[10] Li, C., *et al.*, Experimental study of convective heat transfer in Fe_3O_4-H_2O nanofluids in a grid-shaped microchannel under magnetic field, *Thermal Science*, *27* (2023), pp. 289-289

[11] Bennia, A., Bouaziz, M. N., CFD modeling of turbulent forced convective heat transfer and friction factor in a tube for Fe_3O_4 magnetic nanofluid in the presence of a magnetic field, *Journal of the Taiwan Institute of Chemical Engineers*, *78* (2017), pp. 127-136

[12] Asfer, M., *et al.*, Effect of magnetic field on laminar convective heat transfer characteristics of ferrofluid flowing through a circular stainless steel tube, *International Journal of Heat and Fluid Flow*, *59* (2016), pp. 74-86
[13] Hashemi, A., *et al.*, Direct numerical simulation of transitional flow in a finite length curved pipe, *Journal of Turbulence*, *19* (2018), 8, pp. 664-682
[14] Akar, S., *et al.*, A numerical investigation of magnetic field effect on blood flow as biomagnetic fluid in a bend vessel, *Journal of Magnetism and Magnetic Materials*, *482* (2019), pp. 336-349
[15] Vafeas, P., *et al.*, Effect of the magnetic field on the ferrofluid flow in a curved cylindrical annular duct, *Physics of Fluids*, *31* (2019), 11, 117105
[16] Bakalis, P.A., *et al.*, MHD formulations for the liquid metal flow in a curved pipe of circular cross section, *Computers & Fluids*, *119* (2015), pp. 1-12
[17] Ashjaee, M., *et al.*, Effect of magnetic field on the forced convection heat transfer and pressure drop of a magnetic nanofluid in a miniature heat sink, *Heat and Mass Transfer*, *51* (2015), 7, pp. 953-964
[18] Bezaatpour, M., Goharkhah, M., Convective heat transfer enhancement in a double pipe mini heat exchanger by magnetic field induced swirling flow, *Applied Thermal Engineering*, *167* (2020), 114801
[19] Koo, J., Kleinstreuer, C., A new thermal conductivity model for nanofluids, *Journal of Nanoparticle Research*, *6* (2005), 6, pp. 577-588
[20] Bezaatpour, M., Goharkhah, M., Effect of magnetic field on the hydrodynamic and heat transfer of magnetite ferrofluid flow in a porous fin heat sink, *Journal of Magnetism and Magnetic Materials*, *476* (2019), pp. 506-515
[21] Xuan, Y., *et al.*, Conceptions for heat transfer correlation of nanofluids, *International Journal of Heat and Mass Transfer*, *43* (2000), pp. 3701-3707
[22] Bergman, T., *Fundamentals of heat and mass transfer*, John Wiley & Sons, Hoboken, USA, 2011.
[23] Sha, L., *et al.*, Experimental investigation of convective heat transfer coefficient using Fe_3O_4/water nanofluids under different magnetic field in laminar flow, *CIESC Journal*, *69* (2018), 4, pp. 1349-1356
[24] Nicolaou, L., Zaki, T. A., Characterization of aerosol Stokes number in 90° bends and idealized extrathoracic airways, *Journal of Aerosol Science*, *102* (2016), pp. 105-127
[25] Taibi, R., *et al.*, CFD investigation of internal elbow pipe flows in laminar regime, *IOP Conference Series: Materials Science and Engineering*, *1201* (2021), 1, 012012
[26] Kelidari, M., Moghadam, A. J., Effects of Fe_3O_4/Water Nanofluid on the Efficiency of a Curved Pipe, *Journal of Thermal Science and Engineering Applications*, *11* (2019), 4
[27] Sha, L., *et al.*, The influence of the magnetic field on the convective heat transfer characteristics of Fe_3O_4/water nanofluids, *Applied Thermal Engineering*, *126* (2017), pp. 108-116
[28] Xu, B., *et al.*, Numerical investigation of cavitation suppression in an inducer for water and liquid nitrogen with emphasis on thermodynamic effect, *Journal of the Brazilian Society of Mechanical Sciences and Engineering*, *43* (2021), 212
[29] Fadaei, F., *et al.*, Heat transfer enhancement of Fe_3O_4 ferrofluids in the presence of magnetic field, *Journal of Magnetism and Magnetic Materials*, *429* (2017), pp. 314-323

Submitted: 15.06.2024.

Revised: 26.09.2024.

Accepted: 02.10.2024.